River hydraulic modelling with ICEsat-2 land and water surface elevation

Monica Coppo Frias[1,3], Suxia Liu[2,3], Xingguo Mo[2,3], Karina Nielsen[4], Heidi Ranndal[4], Liguang Jiang[6], Jun Ma[5], and Peter Bauer-Gottwein[1]

[1]Department of Environmental and Resource Engineering, Technical University of Denmark, 2800 Kgs. Lyngby, Denmark
[2]Key Laboratory of Water Cycle and Related Land Surface Processes, Institute of Geographic Sciences and Natural Resources Research/Chinese Academy of Sciences,100101 Chaoyang District, Beijing, China
[3]Sino-Danish Colleage, University of Chinese Academy of Sciences, Beijing 100049, China
[4]Department of Geodesy and Earth Observation, Technical University of Denmark, 2800 Kgs. Lyngby, Denmark
[5]Hydrology Bureau,Yellow River Water Conservancy Commission, Zhengzhou, Henan, 450004, China
[6]School of Environmental Science and Engineering, Southern University of Science and Technology. 1088 Xueyuan Avenue, Shenzhen 518055, P.R. China

Correspondence: Monica Coppo Frias (mcfr@env.dtu.dk)

Abstract. Advances in geodetic altimetry instruments are providing more accurate measurements, enabling satellite missions to hand over useful data in narrow rivers and streams. Altimetry missions produce spatially dense land and water surface elevation measurements in remote areas where in-situ data is scarce, that can be combined with hydraulic/hydrodynamic models to simulate water surface elevation and estimate discharge. In this study, we combine ICESat-2 land and water surface elevation

5   measurements with a low-parametrized hydraulic calibration to simulate water surface elevation and discharge without the need for a rainfall-runoff model. ICESat-2 provides an opportunity to map river cross-section geometry very accurately with an along-track resolution of 0.7 m using the ATL03 product. These measurements are combined with the inland water product ATL13 to calibrate a steady-state hydraulic model to retrieve unobserved hydraulic parameters, such as river depth or roughness coefficient. The low-parametrized model together with the assumption of steady-state hydraulics enables the application of a

10   global search algorithm for parameter calibration at a manageable computational cost. The model performance is similar to that reported for highly parametrized models, with a root mean square error of around 0.41 m. With the calibrated model, we can calculate water surface elevation time series at any chainage point at any time of an available satellite pass within the river reach, and estimate discharge from water surface elevation. The discharge estimates are validated with in-situ measurements at two available gauging stations. In addition, we use the calibrated parameters in a full hydrodynamic model simulation resulting

15   in a RMSE of 0.59 m for the entire observation period.

1 Introduction

Climate change affects the frequency and magnitude of extreme hydrologic events. Rainfall-runoff patterns are changing and with them the frequency of severe floods and droughts which are projected to increase with climate change (Masson-Delmotte V. and B.. (2021)). Understanding how this altered patterns in rainfall-runoff affect water level and inundation along

20   rivers is fundamental for decision support and reliable hydraulic models based on accurate observations are urgently needed. To create such models, measurements on water level and bathymetry are necessary. However, in-situ bathymetric surveys are scarce for remote river systems and such data-sets are typically not in the public domain. Bathymetry estimates based on satellite remote sensing can thus create value for river monitoring and water resources management in inaccessible areas and ungauged river basins.

25   Hydraulic parameters such as riverbed geometry or hydraulic roughness are unobserved in many areas. Riverbed geometry is observable, but measurements require in-situ surveys, while river roughness is not directly observable at the required scales in natural rivers. On the other hand, water surface elevation observations are more accessible and they play a major role in hydrological research. Measurements of water surface elevation are directly related to flooding patterns because flooding occurs when water surface elevation exceeds critical thresholds. In addition, water surface elevation is closely related to discharge

30   in rivers and other hydraulic parameters (Jiang et al. (2017)). During the last 20 years, satellite altimetry has been widely used to monitor water surface elevation, including for inland water bodies. Satellite altimetry has several advantages with respect to traditional survey methods. It provides wide spatio temporal coverage reducing the time and cost of data collection. Missions such as Sentinel-3, CryoSat-2 or Jason-2 have been widely used in inland water monitoring and hydraulic calibration (Tarpanelli et al. (2021); Chen and Wang (2018); Ranndal et al. (2015b); Paris et al. (2016)). However, these missions are

35   limited to wide river streams due to their low spatial resolution (Shen et al. (2020); Paris et al. (2016)) offering an along track resolution around 250-300 m. In contrast, the novel altimetry mission ICESat-2 which has been operating since 2018, offers an along track resolution down to 0.7 m in the photon cloud product ATL03 (Neumann T. A. (2021)). The resolution of ICESat-2 provides an opportunity to measure not only water surface elevation in narrower river streams, but also to map the topography surrounding the river at a high spatial resolution, which can improve the quality in riverbed geometry data-sets for hydraulic

40   simulations.

   Hydrodynamic model calibration requires significant computational resources, since solving the Saint-Venant equations requires short time steps (typically on the order of minutes) resulting in long simulation times for seasonal or multi-year periods. Thus, inverse modeling workflows, where the forward response has to be evaluated at least thousands of times, need model simplifications , especially when global search algorithms are used. Studies such as Jiang et al. (2019) use a distributed

45   bathymetry and roughness along the river channel in a regularized inversion framework using local gradient search methods. A constrained parameter space will greatly help in reducing computation time, therefore, the number of distributed parameters should be limited. Kittel et al. (2021) proposed to use a steady state version of the Saint-Venant equations that significantly reduces computational time in the calibration process, providing a reasonable representation of river channels to be used in a full hydrodynamic simulation.

50   Altimetry missions provide accurate elevation measurements at many cross-over points between satellite ground tracks and rivers, but at low temporal resolution, Cryosat-2, Sentinel-3 and ICEsat-2 provide repeat passes every 369, 27 and 91 days respectively. Altimetry densification is a method that combines intermittent data from different cross-over points into a dense time series at specified points in space. This approach is used to enhance the low temporal resolution of altimetry missions. Studies such as Boergens et al. (2016), Yoon et al. (2013) or Paiva et al. (2015) use kriging interpolation approach, which makes

predictions based on a linear combination of nearby observations. Another approach is interpolating water level observations along the river, using water surface elevation slope, as done by Ranndal et al. (2015a). However, the best estimators of water surface elevation in time and space are hydrodynamic models, which can be derived from altimetry data and respect the physical laws governing flow in open channels (Jiang et al. (2017)). Moreover, calibrated hydrodynamic models are the best tool to define water surface elevation- discharge relationships, where altimetry data can be used to update the states of the hydrodynamic model (Paiva et al. (2013)).

The aim of this paper is to combine ICEsat-2 land and water surface elevation data-sets with river hydraulic modelling. This is an important step towards retrieval of hydraulic parameters that are often unobserved or unobservable at relevant spatial scales such as Manning's roughness or river depth. Hydraulic characterization of river channels enables the conversion of discharge to water surface elevation and vice-versa. This study proposes a method to estimate discharge from ICEsat-2 water surface elevation observations. In addition, the water surface elevation observations and discharge estimations are densified in space and time. With this approach, we produce dense time series and overcome the spatial and temporal sampling limits that characterize altimetry missions.

2 Materials and methods

An overview of the workflow, including different data processing and modeling steps, is presented in figure 1. The method uses two different ICEsat-2 data products as inputs and a steady-state 1D hydraulic model in the inverse hydraulic parameter calibration process. The ATL03 and ATL13 products are processed (see sections 2.1.1 and 2.1.3) to be ingested together with in-situ discharge data in a hydraulic model calibration to estimate river flow depth, roughness coefficient and river bed shape. The calibrated model is used to calculate rating curves relating discharge and water surface elevation and interpolate water surface elevation time series along the river stretch. In addition, the parameter values are used to run a full 1D hydrodynamic simulation.
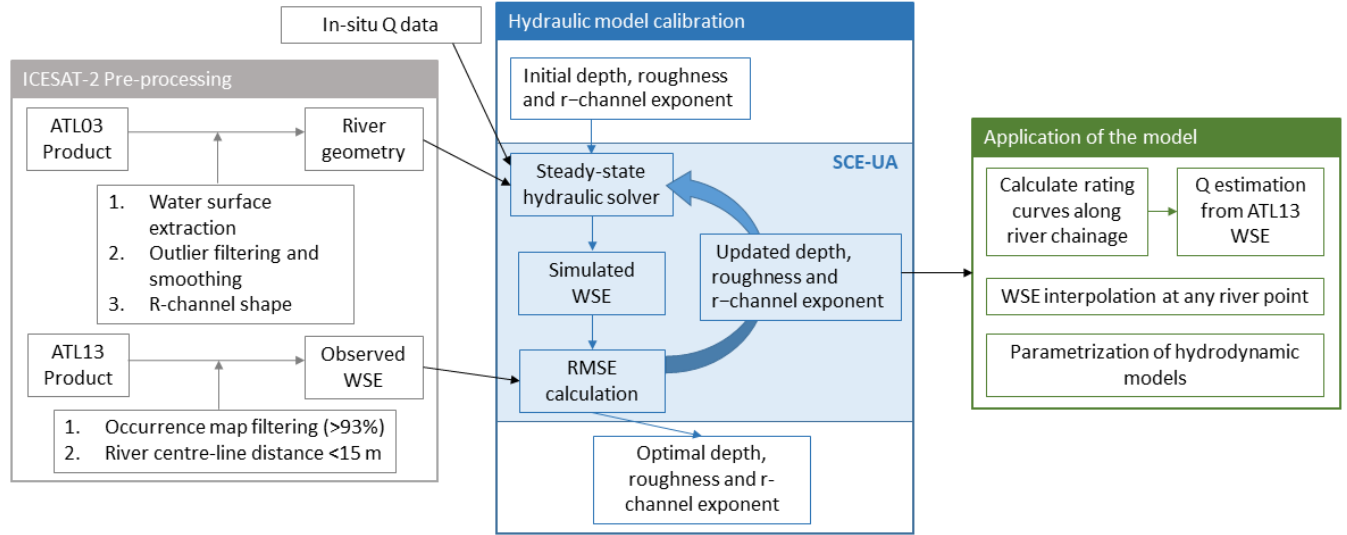
Figure 1. Schematic diagram of the data processing and modelling workflow in this study. The methodology proposes a series of applications from a calibrated model.

2.1 ICEsat-2 land and water surface elevation data processing

2.1.1 ATL03 cross-section processing

The ATL03 photon cloud product is used to define river bed geometry. To ensure that as large a portion of the river bed as possible can be extracted from ICESat-2 observations, only the low-flow season crossings are taken into account, corresponding to the period between November and April. The water surface in the ATL03 data is characterized by a dense cloud of photons. A Gaussian Kernel distribution is used to identify the water surface by taking the peak density value of the distribution. The points between 20 cm from the peak value are also identified as water surface and averaged. The river width is calculated as the along-track extent of the water surface, taking into account the crossing angle between ICESat-2 ground-track and river center line.

To remove outliers from the photon cloud, two different methods are used: firstly, a Hampel filter is applied, in which the Median Absolute Deviation (MAD) is calculated for a sliding window in a 3.5 m ground-track interval. A value will be considered an outlier if it exceeds the MAD. The MAD is defined as in equation 1:

$$MAD = median(X_i - \tilde{X}) \tag{1}$$

with $\tilde{X} = median(X)$. After the Hampel filter, a Median filter is applied for the same 3.5 meters ground-track intervals. The ground-track interval is a "window" that slides entry by entry, and replaces each entry value by the median of the neighboring entries.

Finally, in order to obtain a well defined shape of the river cross-section, a Simple Moving Average (SMA) is calculated for ground-track intervals of 3.5 m.

2.1.2 R-shape geometry for submerged portion

95   In the submerged portion of the channel, the ATL03 product does not detect the riverbed elevation. This product can successfully map bathymetry for clear waters, as shown by Parrish et al. (2019), who present results mapping seafloor bathymery. The portion of the Upstream Yellow river we focus on (see section 2.5), is characterized by fast and turbulent flow, which explains why bathymetry can not be detected by ICESat-2 in this area. To cope with this limitation, the data of the submerged portion is calculated using the approach proposed by Dingman (2007). The shape of the submerged portion depends on a cross-section

100   form exponent r, with $r = 1$ corresponding to a triangle and $r \rightarrow \infty$ corresponding to rectangular shape. The height above the lowest channel elevation, z, is approximated by equation 2,

$$z = Y_m^* \left(\frac{2}{W^*} \right)^r \cdot x^r, \qquad\qquad 0 \leq x \leq W^*/2, \qquad\qquad (2)$$

where Y_m^* is the low flow depth, W^* is the bank width, and x is the horizontal distance from the river center-line.

Figure 2 shows the different processing steps applied to ATL03 data to define the river bed geometry. In the last step, the

105   submerged portion is interpolated, thus for each cross section, there are two free parameters Y_m^* and r that will be estimated in the hydraulic inversion (see section 2.3).
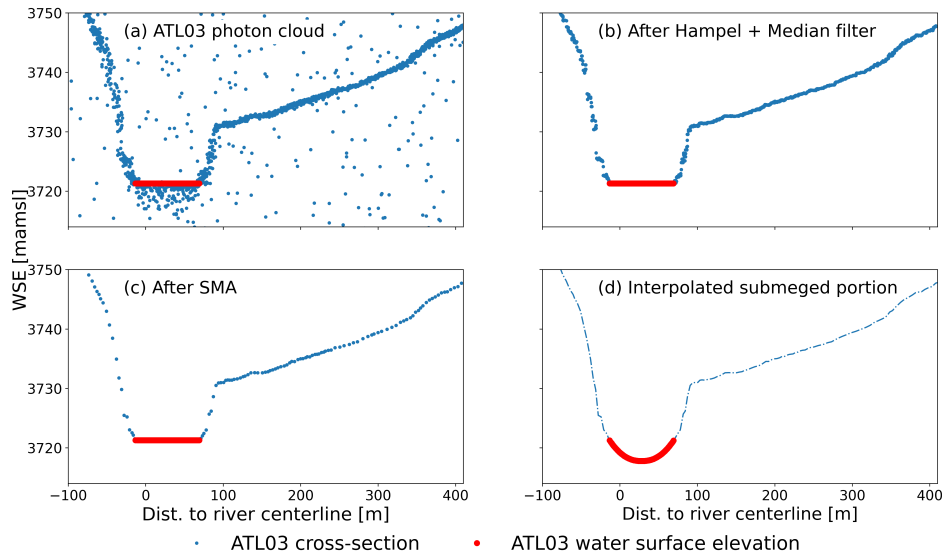
Figure 2. ATL03 photon cloud, where the water surface is identified (a). The outliers are removed using Hampel and Median filter (b). Smoothing of the cross-section with SMA (c), and interpolation of the submerged portion (d).

2.1.3 ATL13 data processing

The model calibration needs an adequate selection of water surface elevation data from ATL13 or other suitable altimetry missions. Radar altimetry missions, such as Cryosat-2 or Sentinel-3 cannot provide high-accuracy measurements in this area

110   due to their low spatial resolution (250-300 m). The river stretch we focus on, has river width varying between 80 meters in

the low flow to few hundred meters in the high flow season. The ATL13 product offers a variable resolution depending on the acquisition date, but it is normally of the order of few meters (Jasinski M. F. and the ICESat-2 Science Team (2021)). This ICESat-2 product offers a variety of data quality flags to discard invalid measurements. In Xu et al. (2021) the following flags are considered for water surface elevation assessments: qf_bckgrd, qf_bias_em, qf_bias_fit, $stdev\_water\_surf$ and

115   $snow\_ice$. These flags control the density of background photons, electromagnetic bias, bias in the fit, standard deviation of water surface elevation and presence of snow or ice. After applying the flags, Xu et al. (2021) recommends an extended outlier filtering method. Moreover, the ATL13 data product presents known issues, such as including land area adjacent to water level or land measurements in the low flow season that need to be considered (Jasinski et al. (2021b)).

    In this study, we first apply the water occurrence map from Global Surface Water Explorer (Pekel et al. (2016)), taking only

120   observations that fall in areas with water occurrence larger than 93%. Taking into account the river delineation extracted from the MERIT database (Yamazaki D. (2019)) (see section 2.6.3), we only consider water surface elevation points that are less than 15 m away from the river center-line. The points that are within 15 m from the river center-line are averaged. In addition, all the water surface elevation measurements within the same acquisition date, that are less than 500 m away from each other, and where the water surface elevation variation is less than 15 times the slope times the distance between observations are

125   averaged.

    We compared the performance of the filtering process with the quality flags, taking the values proposed by Xu et al. (2021), $qf\_bckgrd < 6$, $qf\_bias\_em < 2$, $qf\_bias\_fit < 2$, and constraining the water surface standard deviation, $stdev\_water\_surf$ to 0.5 m. The $snow\_ice$ flag was also applied, with no presence of ice for the area of interest. The results are better when we filter with respect to the river center-line and water occurrence map, than using the ATL13 quality flags. After applying the

130   quality flags only, some of the points that fall on adjacent land area are not removed.

2.1.4 Cross-sections and observation points selection

Cross-sectional data from ATL03 is selected for the available dates in the low flow season. Depending on the acquisition dates, the discharge varies and, accordingly, the reference water surface elevation of the cross-section changes. This can lead to unreasonable variations in the bottom elevation when constant depth is assumed leading into simulation errors. To have a

135   realistic reference bottom level, we take the ATL03 cross-section with the minimum discharge value at the acquisition date from the in-situ data, and calculate the discharge variation between the reference discharge and the discharge for the different ATL03 acquisition dates. The variation of discharge times α, which is a calibration parameter, is added to the corresponding cross-section depth.

    ATL03 and ATL13 variation in water surface elevation for the same acquisition date is calculated to remove possible offsets

140   between the two data-sets. An example of the offset between ATL03 water surface elevation and ATL13 water surface elevation can be seen in figure 3 (e), where the difference between both elevations is about 0.41 m.
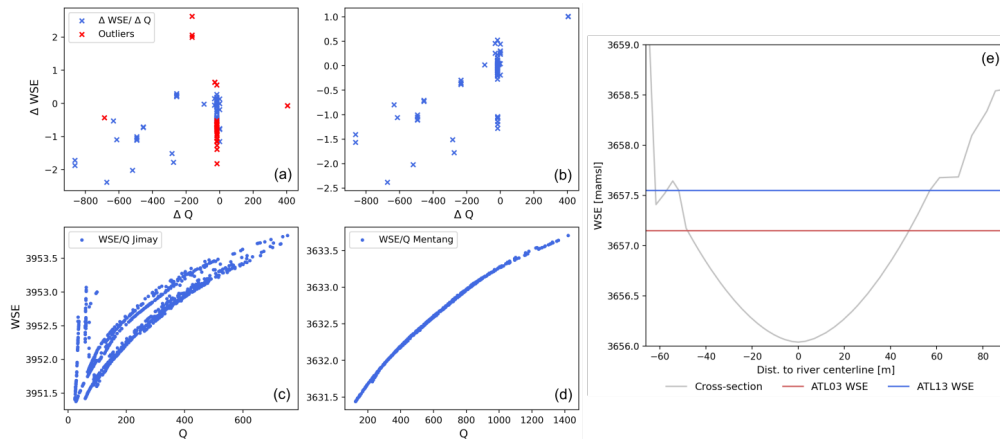
Figure 3. Variation of discharge against water surface elevation from ATL03 and ATL13 (a). Variation of discharge against variation of water surface elevation from ATL03 and ATL13 after correction (b). Rating curve (discharge against water surface elevation) for Jimai gauging station (c). Rating curve for Mentang gauging station (d). Example of mismatch between ATL13 and ATL03 water surface elevation (e).

To detect possible outliers, we compare the discharge variation, ΔQ, between the acquisition date of ATL03 crossing and the one at ATL13 acquisition date. In addition, we check the variation in water surface elevation, ΔWSE, extracted from ATL03 cross-section and the one from the ATL13 product for the same acquisition date at the same chainage point. We expect that

145 the water surface elevation varies accordingly to the discharge variation. In figure 3 (a), we can observe an offset between the discharge variation and the water surface variation, where points with ΔQ close to zero have a ΔWSE around 0.4 to 0.5 m that is related to the mismatch between ATL13 water surface elevation and the reference water surface elevation in the cross-section retrieved from ATL03 product. To correct this offset, the reference water surface elevation from ATL03 is substituted by the one from ATL13 product. In addition, we observed outliers in the Jimai in-situ data rating curve, in which for certain

150 dates, the relation between water surface elevation and discharge does not fulfil a power law (see figure 3, (c)). The outliers we observe for high water surface elevation and low values of discharge correspond to dates in the low flow season, more likely in the months between November and February. Moreover, the rating curve seems to change depending on the year, which contradicts the assumption of stable river bed. The distribution between ΔQ and ΔWSE points in figures 3 (a) and (b) is not related to the anomalies in the Jimai rating curve but is related to the difference between the acquired cross-section data and

155 acquired water surface elevation data, apart from the selected outliers that are removed. The Mentang station does not present these outliers since there is not data available for the low flow period. After inspection, the ATL03 cross-sections acquired in these dates were substituted by a different satellite pass in which the power law is fulfilled.

2.2 1D Hydraulic model

The steady-state hydraulic solver is based on the Saint-Venant equations in steady state. These equations express the mass and

160 momentum balance in an open channel as given by equation 3.

$$q = \frac{\partial A}{\partial t} + \frac{\partial Q}{\partial x} \qquad\qquad \frac{\partial Q}{\partial t} + \frac{\partial}{\partial x}\left(\frac{\beta Q^2}{A}\right) + gA\frac{\partial h}{\partial x} - gA(S_0 - S_f) = 0 \tag{3}$$

The steady-state assumption implies constant discharge over time, hence all time derivatives are zero. The x is the chainage or distance along the channel, h is channel depth, A is the flow cross-sectional area, q is the lateral inflow, Q is the discharge, S_0 and S_f are the bed and friction slopes respectively, g is the gravitational constant and β is the momentum coefficient which is set to 1.

From the steady state solver, we calculate water surface elevation profiles from a given discharge at the downstream point as described in Kittel et al. (2020). The water surface elevation is calculated step-wise at Δx spatial increments and moving upstream along the channel. The equation to solve is presented in 4, which is based on Saint-Venant equations (see Kittel et al. (2020) for the full derivation).

$$RHS(x, h(x)) = \frac{\left(\frac{Q^2}{gA^3}\frac{\partial A}{\partial x} + S_0 - \frac{Q^2}{K^2} - \frac{2Q \cdot q}{gA^2}\right)}{\left(1 - \frac{Q^2}{gA^3}\frac{\partial A}{\partial x}\right)} \tag{4}$$

The model is initialized by calculating the downstream water surface elevation from in-situ discharge using Manning's equation for the local slope value between the two most downstream cross-sections. This value is initialized at 0.0011 m/km and updated at each iteration. Equation 4 is solved explicitly as expressed in 5

$$h_{i-1} = h_i - RHS(x_i, h_i) \cdot \Delta x \tag{5}$$

The chainage grid is defined with step increments of 300 m in between observed cross-sections when the slope is less than 0.20 m/km, for the sections of the river range with steeper slope ($\geq 0.20 m/km$) or areas in which neighboring cross-sections present a significant difference in low flow width, the step increment is reduced to 100 m to avoid instability of the explicit numerical scheme. To make sure that model results are independent of the chosen grid discretization, different forward runs were made for step size down to 50 m, and differences in simulated water surface elevation was shown to be insignificant.

The lateral inflow q is distributed along the chainage proportionally to the contributing area (see fig. 4), taking into account the discharge variations from upstream and downstream in-situ data (see section 2.2.1). The lateral inflow at chainage x is calculated as in equation 6.

$$q = \frac{Q_x - Q_{x-1}}{\Delta x} \tag{6}$$

To calculate the discharge at chainage x, Q_x, we assume the runoff is distributed as the flow accumulation map, proportionally to the contributing area. This relation for discharge is calculated a in equations 7 and 8.

2.2.1 Boundary conditions

The downstream boundary is defined as a free uniform outflow boundary condition (Li et al. (2017)) . This boundary is defined 10 km away from the downstream station, by duplicating the ATL03 cross-section defined closest to Mentang station. To

initialize the steady state solver, a value of water surface elevation at the downstream point is calculated from in-situ discharge
190 values, using Manning's equation.

The lateral inflow boundary is defined assuming that the runoff in the catchment is uniformly distributed, i.e. boundary inflow
is proportional to the increment in contributing area, which is available from the MERIT dataset (see section 2.6.3). Instead
of calculating a rainfall run-off model, we use in-situ discharge measurements at two available stations Jimai (upstream)
and Mentang (downstream) (see section2.5). For the downstream station, Mentang, the available data is between May and
195 November, while for the upstream station, Jimai, there is data available for the whole period. Hence, two possible scenarios
are taken into account:

1. If in-situ observations are available at both upstream and downstream stations, the distributed discharge at chainage point
x is as in 7,

$$Q_x = Q_{up} + \frac{UPA_x - UPA_{up}}{UPA_{ds} - UPA_{up}}(Q_{ds} - Q_{up}) \tag{7}$$

200 2. If only upstream in-situ data is available, which is the case for the low season period (October to May), we consider the
discharge at chainage point x is as in equation 8.

$$Q_x = Q_{up} + \frac{UPA_x - UPA_{up}}{UPA_{up}}(Q_{up}) \tag{8}$$

2.3 Parameter estimation

The objective of the parameter estimation is retrieval of river bed geometry characteristics, i.e. Y_m^* and r (eq. 2) as well as
205 Manning's roughness for each cross-section. To estimate the hydraulic parameters, model calibration is performed for uniform
low flow depth, Manning's roughness, r-shape exponent and a correction factor alpha. The calibration algorithm we use is the
Shuffled Complex Evolution from the University of Arizona (SCE-UA) presented by Duan et al. (1992) and implemented in
Python using Spotpy (Houska et al. (2015)). The SCE-UA is a global optimization algorithm that partitions the parameter space
into complexes. Each complex is evolved independently according to the competitive complex evolution (CCE) presented by
210 Nelder and Mead (1965) and shuffled (re-partitioned) after each evolution to ensure an efficient global search. For the method
to give a better overall performance, the number of complexes is set to $2n + 1$ where n is the number of parameters (Duan
and Sorooshian (1993)), in our optimization algorithm we work with 9 complexes. The objective function is the the standard
deviation of the prediction error between the ATL13 WSE and the simulated WSE, know as the Root Mean Square Error
(RMSE):

$$215 \quad Obj = \sqrt{\frac{1}{N}\sum_{i=1}^{N}\left(WSE_{sim} - WSE_{ATL13}\right)^2} \tag{9}$$

The low flow depth varies between 1.5 and 2.5 m and its initial value is 2 m, the manning roughness varies between 0.027 and 0.06 $s/m^{1/3}$ and it is initialized at 0.031 $s/m^{1/3}$, the r-shape exponent varies between 1.5 and 2.7 and it is initialized at 1.8 and the correction factor alpha varies between 0.0005 $m/m^3/s$ and 0.003 $m/m^3/s$ and it is initialized at 0.002 $m/m^3/s$.

220   The sensitivity of the parameters in the model calibration is calculates using FAST (Fourier amplitude sensitive test) proposed by Saltelli et al. (1999).

2.4   Application and use cases

2.4.1   Water surface elevation densification and discharge retrieval

The calibrated model reproduces water surface elevation-discharge relationships in the form of rating curves. We produce a
225   series of rating curves along the river stretch for a given downstream discharge value to create a look-up table between river chainage, water surface elevation and discharge. This relation can be used for different applications:

1. Densification of water surface elevation: This is the aim of several studies, which use different methods to interpolate altimetry water surface elevations like Kriging methods (Boergens et al. (2016), Yoon et al. (2013)) or interpolation using water level slope (Ranndal et al. (2015a)). In our case, we use the calibrated 1D hydraulic model to calculate water
230   surface elevation along the river stretch. Using ATL13 observations at different acquisition times, we can predict water surface elevation at any river point using the calibrated model.

2. Discharge retrieval: The calibrated model can be used to convert ATL13 water surface elevation observations into estimates of river dicharge using water surface elevation-discharge relation. At any time of ICEsat-2 acquisitions or any other type of altimetry data, we can ingest a observation of water surface elevation to produce discharge estimate in any
235   point of the river stretch using the estimated rating curves from the 1D hydraulic model.

2.4.2   Parametrization of HD models

The optimal parameters from the 1D hydraulic calibration can subsequently be transferred to a full hydrodynamic model simulation if predictions of dynamics of discharge and water surface elevation are of interest. We use MIKE Hydro River to simulate the river hydrodynamics in the transient state using a dynamic wave solver of the 1D Saint-Venant equtions. To run the
240   hydrodynamic model we use daily in-situ discharge data as upstream boundary for a period of 3 years. MIKE Hydro River uses the calibrated cross-sections to get information on calibrated channel geometry and optimal Manning's roughness coefficient. The runoff increment is distributed according to the contributing area which is obtained from the river delineation.

2.5   Demonstration case: upstream Yellow River

The Yellow river is the second longest river in China and the sixth longest in the world. The total length of the river is around
245   5464 km and it has a drainage area of about 795.000 km^2. It rises in the Qinghai province of western China, in the Bayan Har

mountains. The high flow season occurs during the rainy period, between June to October, and the low flow season is between November to May.

Our focus is the Upstream Yellow River (see figure 4), starting in its source in the Bayan Mountains and flowing to Thangnaihai, where elevations are above 3600 m above mean sea level. The total basin area is about 386.000 km^2. We select a
250 river stretch between Jimai and Mentang, with a distance along the channel about 300 km. Jimai is located at $33°46'12''N$, $99°39'25''E$ at an elevation about 3950 meters above mean sea level, and Mentang is located at $33°46'12''N$, $101°2'60''E$ at an elevation about 3630 meters above mean sea level. The river section just downstream of Jimai is characterized by alluvial plains for about 50 km and becomes narrower with steep cliffs lining both sides of the river until it reaches Mentang. This river stretch is characterized by a narrow river width , between 80-180 meter in low flow season with curved structures, making it a
255 good example to demonstrate the ability of ICEsat-2 data in narrower river streams.
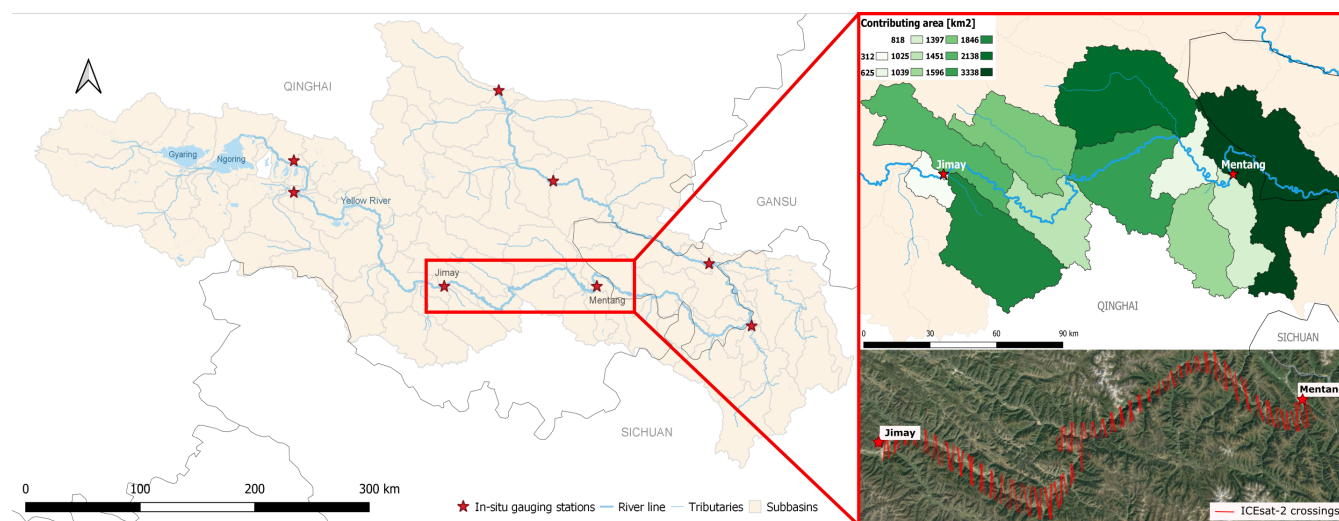
Figure 4. Area of interest in Upstream Yellow river and in-situ gauging stations. Calibration is performed for the river reach between Jimai and Mentang (zoom). The top right image represent the catchment area along the river range. The bottom right image shows the ICEsat-2 crossings available in the river stretch.

2.6 Data

2.6.1 Icesat-2

ICESat-2 data is acquired from the National Snow Ice Data Center (NSIDC) portal and the National Space Institute, Technical University of Denmark (DTU Space) database for the period between 31/10/2018 to 02/04/2021.
260 Two different product levels are used: ATL03, ATLAS/ICESat-2 L2A Global Geolocated photon Data and ATL13, ATLAS/ICESat-2 L3A Along Track Inland Surface Water Data, both having a temporal resolution of 91 days.

ATL03 product has an along-track resolution of 70 cm and provides the geolocated photon event down-linked from ATLAS. The signal photon events are distinguished from the background events by calculating the signal to noise ratio. We use this product to map the land topography of the river cross-section and measure hydraulic parameters such as river flow width and water surface elevation as explained in section 2.1.1.

ATL13 product (Jasinski et al. (2021c)) provides inland water surface elevation with an ensemble error of 6.1 cm per 100 inland water photons (Jasinski et al. (2021a)) . The along-track resolution of this product varies, but is typically of the order of few meters. We use this product to extract mean water surface elevation at located river crossings, for the steady state model calibration. The ATL13 data is prepared for the period between 31/10/2018 to 21/09/2020, to cover the period for which in-situ discharge data is available. In addition, there is a validation data-set in the period from 13/12/2020 to 19/10/2021 in which there are in-situ observations available.

2.6.2 In-Situ data

In situ observations from Jimai and Mentang gauging stations were kindly provided by the Yellow River Conservation Commission (YRCC). The available data covers the period between 10/05/2018 and 21/09/2020. Discharge data at both stations is used as boundary conditions for the steady-state hydraulic model, that simulates water surface elevation along the river reach from given discharge. Jimai station provides data for both low flow and high flow season, while Mentang station is missing the data for the low flow season. Data from the period between 13/12/2020 to 19/10/2021 is available to validate the model.

2.6.3 Ancillary datasets

A 3-arcsec Digital Elevation Model (DEM), flow accumulation map and flow direction map are downloaded from MERIT global database (Yamazaki D. (2019)). A conceptual river basin model is developed, in which the major runoff generating catchments are identified at the main tributaries of the river range. TauDEM is used to delineate the river network and catchments with the information extracted from MERIT database, and the conceptual model (Yamazaki D. (2019)). The river delineation is used as reference for the river center-line when defining river cross-sections. The chainage of the river is generated from the river delineation with steps of 10 m, referenced to Lake Eling, close to the river source in Bayan Har mountains. Water occurrence map is downloaded from the Global Surface Water Explorer (Pekel et al. (2016)). The water occurrence is used to filter the water surface elevation observations from ATL13.

3 Results

3.1 ICEsat-2 data processing

3.1.1 ATL03 cross-sections processing and selection

The cross sections are visually inspected to identify if the land and water topography are well defined, and there are no signs of cloud formation or weather effects. The strong beam and weak beam data, separated by 90 m, were observed to behave

differently depending on the acquisition date. For the cases in which the strong beam signal was very strong, the data can present noise that complicates the processing steps, in this case the weak beam crossing is selected. For acquisitions with weaker signal, the topography is better mapped by the strong beam signal. 80 ATL03 cross-sections are selected, which define

295   the river bed geometry along the river reach between Jimai and Mentang (see figure 5 bottom), including measurements of land elevation of the dry portion of the riverbed. Measurements are provided every 3.5 to 20 m. Closely spaced cross-sections are removed to reduce the computational cost of the model, since only cross-sections that are more than 500 m away provide meaningful information. In areas with scarce ICESat-2 data, there can be a separation between cross-sections up to 10 km. The gaps in the data at the scale of our investigation are mostly due to the poor quality in acquisitions, in the period in which

300   weather conditions are having an impact in ICEsat-2 observations. For the river stretches with little cross-section information, we interpolate cross-section in between using MIKE Hydro cross-section module, however the model quality might be likely worse here.
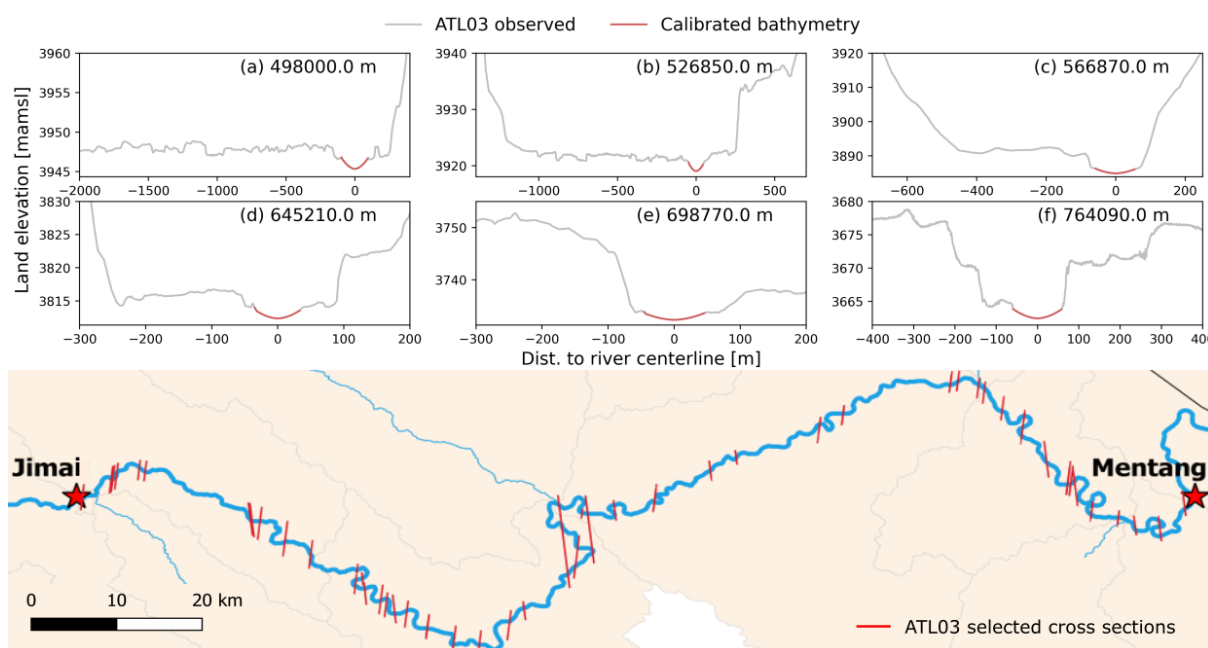
Figure 5. Top: Examples of cross section geometry after calibration, where the majority of points correspond to ATL03 observed data. Bottom: ATL03 selected cross-sections for river hydraulic calibration. 80 cross-section were selected after processing described in section 2.1.1.

    The top panel of figure 5 gives examples on the cross-section geometry measured with ATL03 together with submerged portion that is not observable and has been calibrated. These cross-sections give quite a reasonable representation of the river

305   geometry. An advantage of the method is that most of the cross-section points are from observed data, since the data is selected for the low flow season. This gives a more accurate representation of the hydraulic geometry. In figures 5 (a) and (b), which

correspond to the most upstream part, we can observe the presence of floodplains with braided structure of few kilometers, while the rest of the stretch has a confined structure.

3.1.2   ATL13 water surface elevation processing

310   Initially, we use data from 236 ATL13 crossings which corresponds to 3199 water surface elevation points, illustrated by red crosses in fig 6. After processing the data as explained in section 2.1.3, we get 81 water surface elevation observations that will allow our model to run at a lower computational cost, illustrated by the blue dots in figure 6. The processing steps provide a good sample of water surface elevation observations, with good spatial coverage of the entire river range. Moreover, the temporal coverage of the data-set includes low flow and high-flow season observations, with a slight predominance in the low

315   flow season, that is related to the quality of ICESat-2 data for each period. The filtering criteria are not biased against high flow season observations.
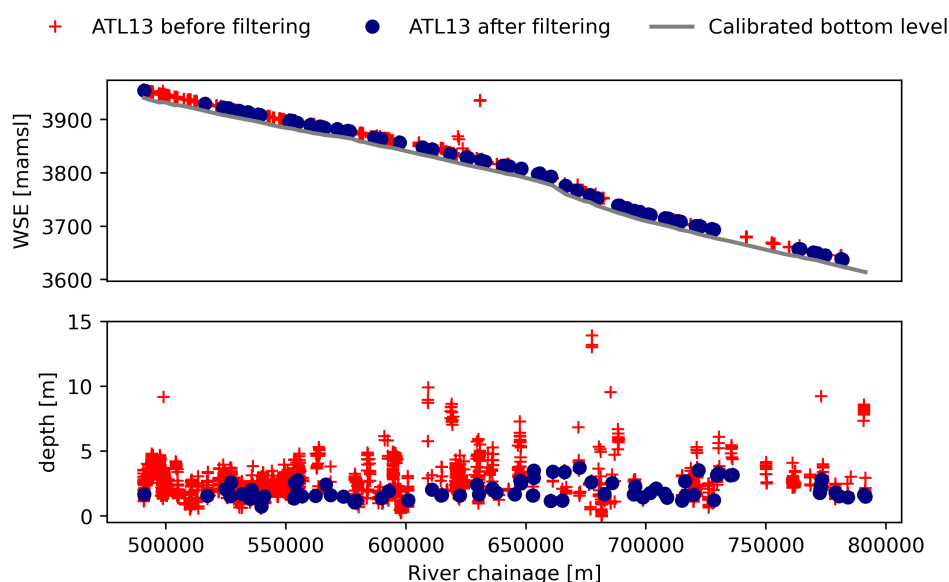
Figure 6. Top: ATL13 data before filtering corresponding to 236 ICESat-2 crossings. Bottom: ATL13 data before processing provides 3199 observation points from 236 different ICEsat-2 crossings. ATL13 data after filtering and processing, corresponding to 81 water surface elevation points.

3.2   Calibration using ICESat-2 observations

The calibration is performed against ATL13 water surface elevation observations for uniform low flow depth and Manning's roughness. A forward run of the model takes 39 seconds and the hydraulic model calibration converges after 1000 runs and

320   runs 500 more times after convergence. Each iteration includes individual runs for 29 different discharge classes, that group the water surface elevation observations by discharge value in the corresponding acquisition date. The minimum RMSE value of the calibration is taken as the optimal value, and results can be seen in table 1. The root mean square error is 0.41 m, which

overall is in good agreement with previous studies (Kittel et al. (2020), Jiang et al. (2019)) considering the low parametrization of the model, which considers uniform depth and roughness. The most sensitive parameters in the FAST sensitivity analysis

325 are Manning's roughness and low flow depth. The optimal parameters estimate are not close to the a priori interval boundaries, which indicates the parameter constraint was well defined. The most correlated parameters are roughness and depth as seen in figure 7.

To study the uncertainty of the model we use a Bayesian uncertainty analysis, Differential Adaptive Metropolis (DREAM) algorithm proposed by Vrugt (2016). This algorithm creates a posterior sampling in the parameter space, from which we take

330 the 10 % best model runs to create the posterior distribution.

Table 1. Steady state solver calibration results for uniform values along the river stretch. The root mean square error (RMSE) is minimized. The sensitivity analysis is performed with FAST. The uncertainty of the parameters is calculated with DREAM.

	Calibrated parameter	FAST sensitivity	DREAM uncertainty
RMSE [m]	0.414		
Manning's n [s/$m^{1/3}$]	0.02927	0.58	±13%
depth (Y_m^*) [m]	1.388	0.884	±11.7%
r	1.785	0.072	±28.6%
$\alpha[m/m^3 s^{-1}]$	0.0019045	0.092	±18.4%
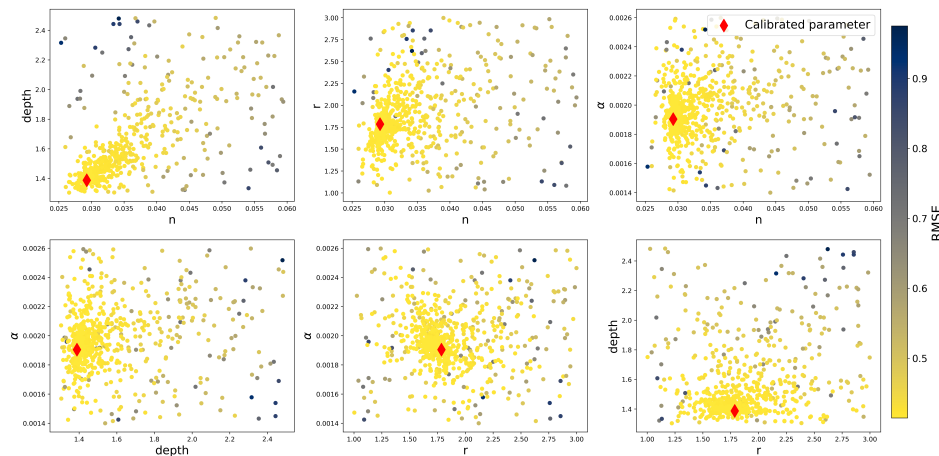
Figure 7. Sampling pattern and model performance during calibration. The objective function is lowered during calibration.

Figure 8 compares the simulated depth (simulated water surface elevation minus calibrated bottom level) and the ATL13 depth (ATL13 water surface elevation minus calibrated bottom level). Overall, the simulated WSE corresponds to the ATL13

wse with a deviation below 1 meter (fig. 8 right). The larger errors are found for selected observations in the downstream area and for observations between chainage 650000 m and 680000 m (fig. 8 left).
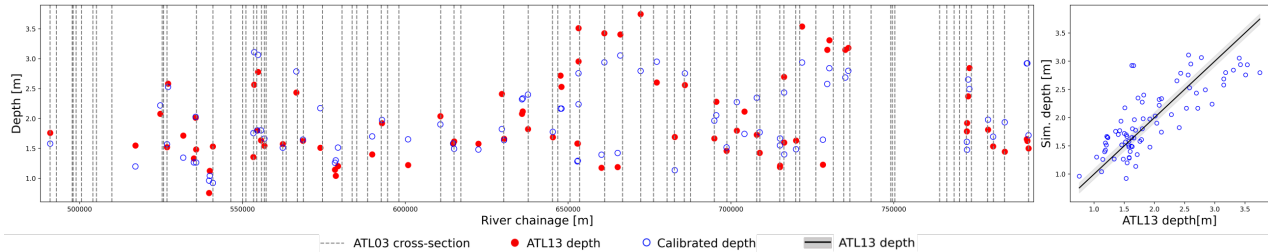
Figure 8. Left: Calibrated longitudinal profile using the steady state solver for uniform depth between Jimai and Mentang. The depth is calculated as the difference between water surface elevation and calibrated bottom level. Right: Simulated vs. ATL13 depth, the shaded area correspond to the mean standard deviation in the ATL13 product, extracted from the flag $stdev\_water\_surf$.

3.2.1 Validation of the model calibration

The validation data consists in ATL13 observations for the period between 13/12/2020 and 19/10/2021 in which in-situ discharge is available are ingested in the calibrated hydraulic model. Whit the validation data, the RMSE of the model is 44.3 cm, which is in good agreement with the calibration RMSE. The error of the validation data can be seen in figure 9. The deviation from the ATL13 depth goes up to 1.5 m (fig. 9 left). We observe again that a larger error is present between chainage 650000 and 680000 m (fig. 9 right) as previously seen in the calibration data.
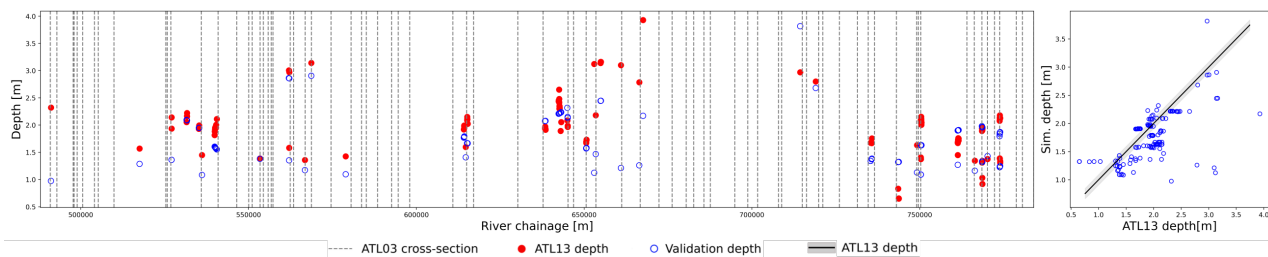
Figure 9. Left: Validation longitudinal profile using the steady state solver for uniform depth between Jimai and Mentang. The depth is calculated as the difference between water surface elevation and calibrated bottom level. Right: Simulated vs. ATL13 depth, the shaded area correspond to the mean standard deviation in the ATL13 product, extracted from the flag $stdev\_water\_surf$.

3.2.2 Rating curves along the river stretch

The rating curves define the relation between water surface elevation and discharge along the river range. Rating curves depend on hydraulic characteristics of the channel, so an accurate parametrization is necessary. The relation water surface elevation-discharge generally follows a power law.

We calculate rating curves every 50 m from the calibrated hydraulic model. This defines a look up table relating discharge, WSE and river chainage. Examples of rating curves in the look up table are illustrated in figure 10, where the flow depth, calculated as simulated WSE minus calibrated bottom level, is compared to the discharge. The calculated rating curves follow a power law, we can also see that for the more upstream point, 491020 m, the discharge values are lower than the ones more downstream.
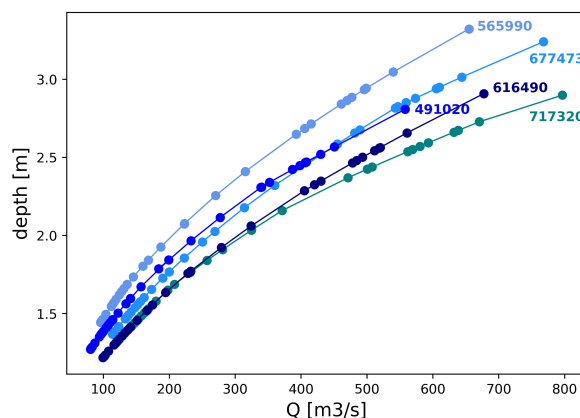
Figure 10. Examples of simulated rating curves relating water surface elevation and discharge at different chainage points.

Note that for the relation at chainage 565990 m, the increase in flow depth is larger than for the rest of examples. This effect is produced due to the narrower river width at this river location, that produces and increase in flow depth for the same discharge values. This is a clear example of the river geometry effect in building WSE-discharge relationships.

3.2.3 Validation of discharge estimation and demonstration of the model use

The results of the validation are presented as the percentage of flow exceedance for a given discharge value and are compared with in-situ data (fig. 11, a) and b)). The estimated discharge values are for selected ATL13 water surface elevation observations. The validation data-set, corresponding to the period from 13/12/2020 to 19/10/2021, is ingested together with the calibration data in the hydraulic model to interpolate the corresponding discharge at the time of acquisition at a given river location (Jimai and Mentang gauging stations). The percentage of flow exceedance for the estimated discharge is in good agreement with the in-situ data. For Mentang station (fig. 11, b)), the discharge values are between 400 to 300 m^3/s 60 to 80 % flow exceedance, while the simulated data is between 350 to 250 m^3/s, which is a considerable large difference. In the simulated discharge we are also calculating low flow values that are missing in the in-situ measurements, which explains this mismatch.

The estimated discharge for Jimai station has a median absolute error around 55 m^3/s while for the downstream station, Mentang, the absolute median error is about 120 m^3/s (fig. 11 c). This difference in median absolute error is again explained by to the lack of low flow in-situ observations for the Mentang station, the error is only calculated in the high flow season.
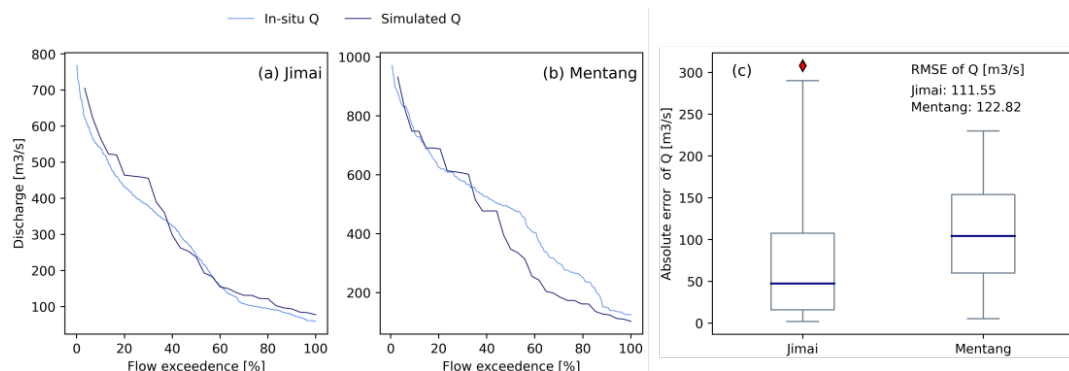
Figure 11. Left: Simulated discharge vs in-situ measured discharge for Jimai (a) and Mentang (b) stations. Right: Absolute error between simulated Q and observed Q. The RSME for the discharge at Jimai and Mentang is also calculated.

Figure 12 shows examples of water surface elevation ((a), (c) and (e)) and discharge ((b, (d) and (e)) time series for 3 different
360 river locations: at chainage 491020 m, 565990 m and 717320 m. The results are interpolated from ATL13 observations using the water surface elevation-discharge relation at the selected river locations. In-situ measurements for water surface elevation to compare with the simulated values are not available.
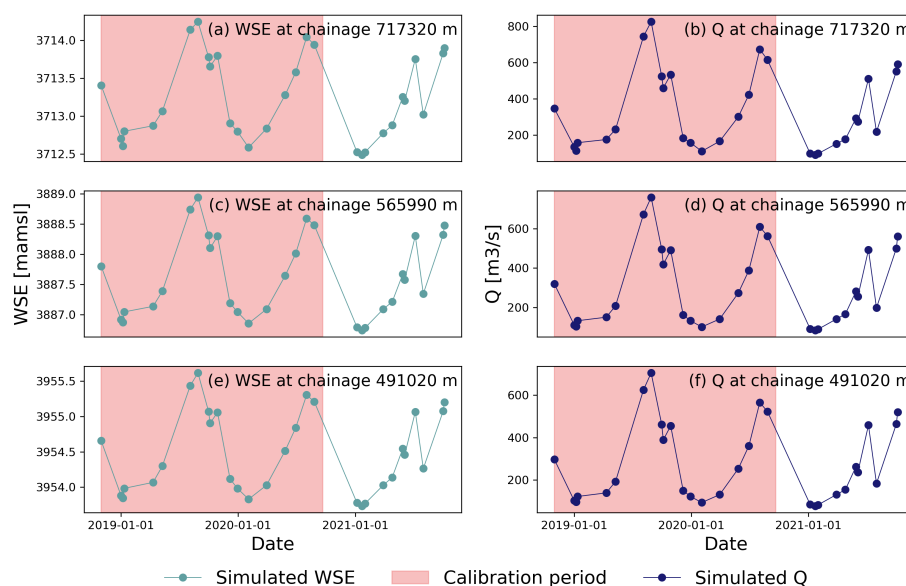
Figure 12. Simulated water surface elevation (a),(c) and (e) and simulated discharge (b), (d) and (f) at selected chainage points.

3.2.4 Parametrization of HD model

The calibrated Manning's roughness, together with the calibrated cross-sections are used in MIKE Hydro river to run a full hydrodynamic model simulation. The model runs in a grid with 1006558 grid points for 2 minutes time-steps and 100 m distance. We define a boundary condition at the upstream cross-section with input discharge from Jimai in-situ data, and a downstream boundary at the synthetic cross-section relating discharge and stage. We use the dynamic wave solver that corresponds to the full 1D Saint-Venant equations. Figure 13 (a) compares the simulated depth by MIKE Hydro and ATL13 depth (water surface elevation minus calibrated bottom level). The simulated depth seems to be underestimated in most of the cases, and the maximum deviation from the ATL13 depth is around 1.7 m. The RMSE is 0.59, which is in good agreement with the results from the steady state solver.

Figure 13. (a) MIKE Hydro simulated depth vs. ATL13 observed depth. The shaded area correspond to the median std. deviation of the ATL13 observations, taken from the flag $stdev\_water\_surf$. (b) Simulated water surface elevation from the state state solver and MIKE.

Figure 13 (b) presents the water surface elevation time series at chainage 491020 m simulated from MIKE and from the steady state solver. The time series represent the seasonal variation fairly good. The simulated values from the steady state solver looks to be above the ones from MIKE simulation. This was also observed when we compare the simulated depth with the observed ATL13 depth (fig. 13 (a)), which makes sense if we take into account that the simulated water surface from the steady state solver is directly derived from ATL13 observations, while the simulated MIKE water surface elevation is derived from discharge observations.

4 Discussion

365

4.1 ICESat-2 data selection

ICESat-2 data provides valuable information for river hydraulic modelling. The ATL03 product gives accurate river geometry measurements. The low flow river width could be retrieved from this product together with measurements of the river dry portion. This is an advantage with respect to other studies in which satellite altimetry could only be used in wider river streams

370 (Lettenmaier et al. (2015), Jiang et al. (2019), Kittel et al. (2020)). The processing of the ATL03 photon cloud data-set provides a well defined shape of the river cross-section, removing background noise and outliers.

Accurate water surface elevation observations are very important in the calibration process. The ATL13 product gives a well distributed sample both in space and time of water surface elevation data. However, several outliers are present, which need a closer look. Besides the quality flags that the product provides, an outlier filtering process was defined based on the water

375 occurrence and river center-line. Applying these two criteria, the main outliers were successfully removed without rejecting good quality observations. There is no need to use the quality flags if we use the proposed outlier filtering method.

The main drawback of ICESat-2 data, is the inability to operate in all weather conditions, since laser altimeter cannot penetrate thick clouds. This creates gaps in the cross-section data of up to 10 km. However, future acquisitions on the corresponding ground tracks can be used to fill these gaps.

380 ## 4.2 Model performance

We presented a uniform flow depth and roughness calibration against ATL13 water surface elevation. The steady state assumption and low parametrization with only 4 calibration parameters, makes the model converge fast using a global search algorithm. The RSME value of 0.41 m was quite satisfactory with respect to other studies which used distributed depth calibration. Indeed, Jiang et al. (2019) obtained a RMSE between 0.72 and 1.6 m using combination of altimetry data-sets. Kittel

385 et al. (2020) presents RMSE between 0.61 and 0.89 m using Cryosat-2 observations only. The most sensitive parameters to the calibration were the roughness coefficient and the low flow depth, while the cross-section form exponent and correction factor had a lower impact. The value of the cross-section form exponent is most uncertain, however changes in this value do not introduce large changes in the model. Additionally to the uniform depth calibration, we attempted to calibrate distributed depth models, that did not improve the RMSE. The test was made for 5 and 10 uniform distributed depths along the river range

390 with uniform Manning's roughness. Defining more parameters in the model increases the computational cost significantly and convergence could not be reached in some cases. We observed a larger error between simulated and observed depth between chainage 650000 and 680000 m, that was not removed when calibrating distributed depths. The water surface elevation in this area seems underestimated for high flow observations and over estimated for low flow observations.

A validation data-set for a 10 month period is used, in which the RMSE is 0.44 m, in good agreement with the calibration

395 data. The same larger error were observed between chainage 650000 and 680000 m.

In addition, we ran calibrations using 8 and 16 distributed Manning's roughness, where the RMSE improves to 0.377 and 0.365 m respectively. However, when evaluating the validation data, the RMSE for 8 and 16 distributed roughness is 0.445 and 0.425 m respectively (see appendix A). The first case is an indicator of over-fitting in the model. Increasing the distributed roughness coefficient to 16 reduces the RMSE in few centimeters, but the computational cost of the calibration increases

400 significantly.

Overall the model performance is satisfactory compared to previous studies, with the added value of being a low parametrized model. In addition, the steady assumption reduces significantly the simulation time, that took 1h and 15 min for a period of 3

years in a full 1D hydrodynamic simulation, compared with the 39 seconds of steady state forward run for all the discharge classes. These two factors make the convergence of the calibration process quite fast.

4.3 WSE densification and discharge estimation

Satellite altimetry provides accurate elevation measurements at the cost of temporal resolution. To create water surface elevation and discharge time series, interpolation of water surface elevation is needed. We use the calibrated hydraulic model to create water surface elevation-discharge relationships in the form of rating curves along the river stretch that makes possible the interpolation of water surface elevation and estimation of discharge at any point in the river for a given ATL13 water surface elevation observation.

In figure 11 we compare the estimated discharge with the available in-situ discharge at Jimai and Mentang stations in % of flow exceedence. The estimations, which looks reasonably close. Examples of interpolated wse and discharge at different chainage points are also provided in figure 12. These results could not be compared with in-situ observation, since this areas are uninformed. With the method we present, the interpolation can be made for the available ICESat-2 acquisitions, which also need processing and outlier removal. It is important to note, that for every river point, ICESat-2 crosses at the same exact point every 91 days, while for the interpolated time series we have up to 3 valid values per month.

Observations from other altimetry missions such as Cryosat-2 or Sentinel-3 are challenging to incorporate in the model, since the flow width is smaller than the along-track resolution of these missions.

4.4 Parametrization of HD models

The calibrated parameters were included in MIKE Hydro River to run a full hydrodynamic model using the dynamic wave solver. The model is numerically stable defining 2 minutes time steps and 100 m distance steps, creating a grid with 1006558 points. The model simulation takes 1 hour 15 minutes to finish. If we compare this running time with the 39 seconds of a forward run in the steady state solver, we can clearly see that a full hydrodynamic simulation is not suitable for calibration. The results presents a larger RMSE of 0.59 m with respect to the RMSE using the steady state solver of 0.41 m. Figure 13 shows that most of the simulated depth are underestimated. The difference in the simulation performance between the steady state calibration and the full hydrodynamic model can be related to the simplification made by the steady state assumption.

5 Conclusions

In this study we present a method for river hydraulic parameter calibration that can be used to estimate discharge and densify altimetry observations. The main novelty of the method is the incorporation of observed cross-sectional geometry from ICESat-2 ATL03 product, that is able to perform in narrow rivers with flow width below 100 m and to map the river dry portion. Previous altimetry missions such as Cryosat-2, Sentinel-2 or Jason-2 did not provide such measurements due to its lower resolution .

The hydraulic model calibration is performed against ATL13 water surface elevation observations. The model has a low parametrization, that together with the steady state assumption makes the calibration converge fast. The resulting RMSE is of

0.41 m, and of 0.44 m when using the validation data-set. These values are in good agreement with previous studies that used

435   larger parametrization. The calibrated model provides estimations of water surface elevation and discharge along the entire
river stretch for a given ATL13 water surface elevation observation. The estimated discharge at Jimai and Mentang is in good
agreement with the in-situ discharge measure at the gauging stations, with an absolute error of 55 m^3/s at Jimai and 120 m^3/s
at Mentang.

The methodology has demonstrated the value of ICESat-2 in hydrological studies, which performs better than previous

440   altimetry missions that were limited to wide river streams. Using a simplified hydraulic model, with steady state assumption
and low parametrization we achieve good results at a reduced computational cost than full 1D hydrodynamic models.

Appendix A: Distributed Manning's roughness calibration

The appendix includes the result of the distributed Manning's roughness calibration and compares it with the uniform calibration results.
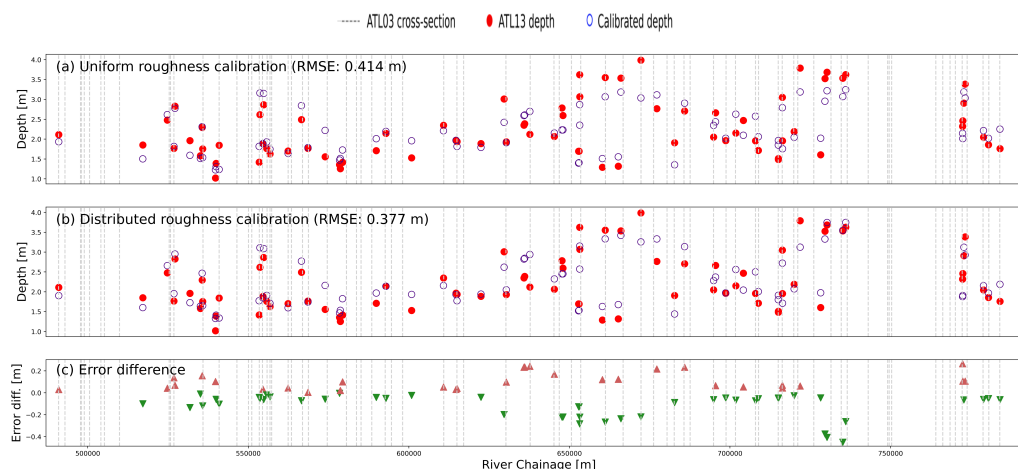
Figure A1. Uniform depth calibration (a) compared with distributed roughness calibration (b) for 8 Manning's roughness and error difference between the uniform calibration and the distributed calibration (c).
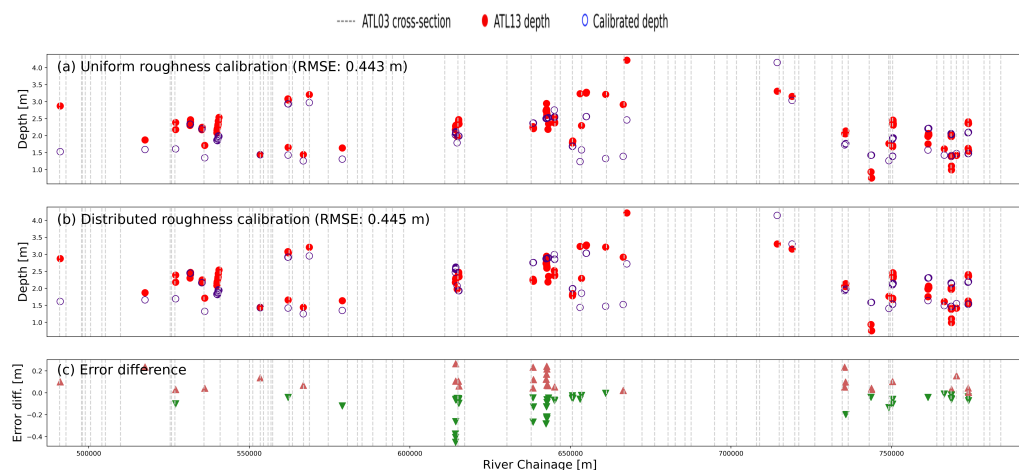
Figure A2. Validation data error for uniform depth calibration (a), distributed roughness calibration for 8 Manning's roughness (b) and error difference between the uniform calibration and the distributed calibration (c)
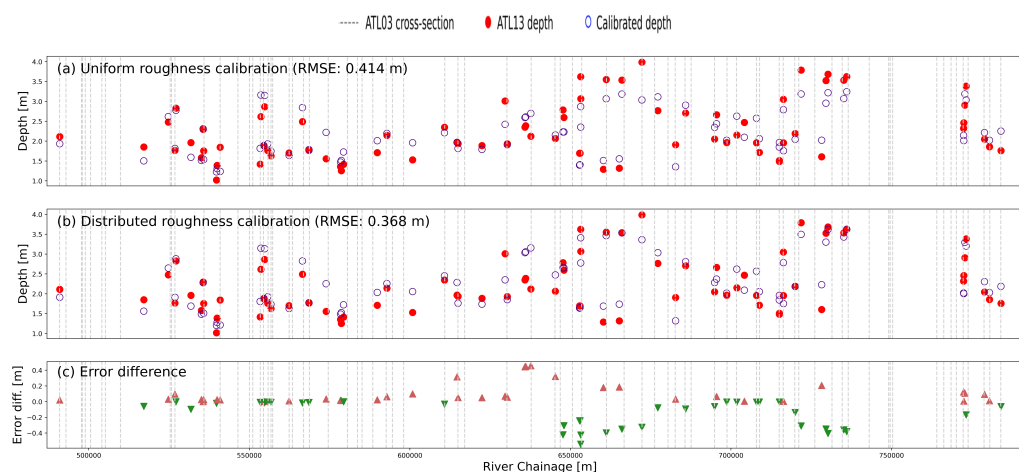
Figure A3. Uniform depth calibration (a) compared with distributed roughness calibration (b) for 16 Manning's roughness and error difference between the uniform calibration and the distributed calibration (c).
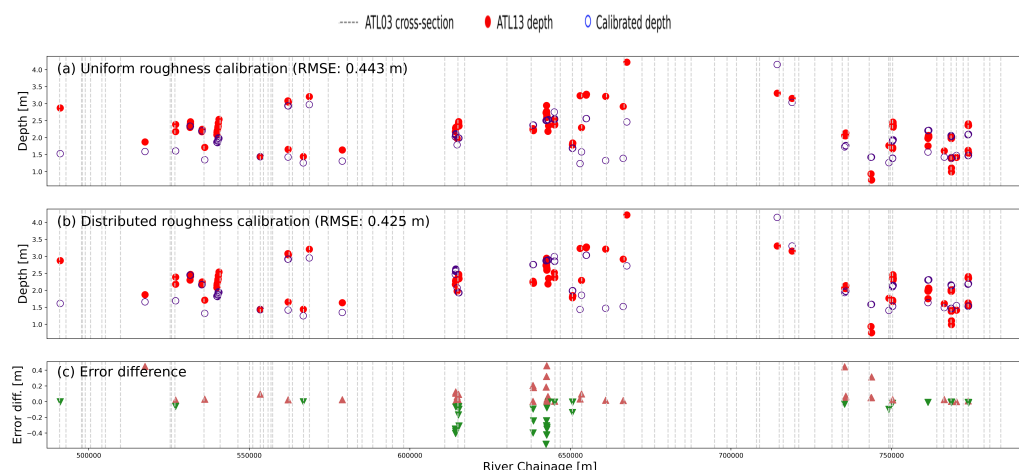
Figure A4. Validation data error for uniform depth calibration (a), distributed roughness calibration for 16 Manning's roughness (b) and error difference between the uniform calibration and the distributed calibration (c)

445 *Code availability.* The code for the 1D hydraulic model and processing of ICESat-2 data can be found on Zenodo (DOI: 10.5281/zenodo.6570492).

Data availability. ICESat-2 data is freely available from the National Snow and Ice Data Center (NSIDC) on https://nsidc.org/data/icesat-2/data-sets0. The MERIT DEM, flow accumulation map and flow direction map can be downloaded from http://hydro.iis.u-tokyo.ac.jp/ yamadai/. The flow accumulation map can be obtained from the Global Surface Water Explorer portal (https://global-surface-water.appspot.com)

450 *Author contributions.* All authors contributed. extensively to this paper.

Competing interests. The authors declare no conflict of interest.

Acknowledgements. The first author is supported by the Sino-Danish Center (SDC). This study is part of three bigger initiatives: CNWaterSense funded by Innovation fund Denmark (no. 8087-00002B), Ministry of Science and Technology of China-National Key Research and Development Program of China (no. 2018YFE0106500) and Hydrocoastal funded by ESA (https://eo4society.esa.int/projects/hydrocoastal/).

References

Boergens, E., Buhl, S., Dettmering, D., Kluppelberg, C., and Seitz, F.: Combination of multi-mission altimetry data along the Mekong River with spatio-temporal kriging, Journal of Geodesy, pp. 1–16, https://doi.org/10.1007/s00190-016-0980-z, 2016.

Chen, L. and Wang, L.: Recent advance in earth observation big data for hydrology, Big Earth Data, 2, 86–107, https://doi.org/10.1080/20964471.2018.1435072, 2018.

Dingman, S.: Analytical Derivation of At-a-Station Hydraulic-Geometry Relations, Journal of Hydrology - J HYDROL, 334, 17–27, https://doi.org/10.1016/j.jhydrol.2006.09.021, 2007.

Duan, Q., Sorooshian, S., and Gupta, V.: Effective and efficient global optimization for conceptual rainfall-runoff models, Water Resources Research, 28, 1015–1031, https://doi.org/https://doi.org/10.1029/91WR02985, 1992.

Duan, Gupta, V. and Sorooshian, S.: Shuffled complex evolution approach for effective and efficient global minimization, Journal of Optimization Theory and Applications, 76, 1573–2878, https://doi.org/https://doi.org/10.1007/BF00939380, 1993.

Houska, T., Kraft, P., Chamorro-Chavez, A., and Breuer, L.: SPOTting Model Parameters Using a Ready-Made Python Package, PLOS ONE, 10, 1–22, https://doi.org/10.1371/journal.pone.0145180, 2015.

Jasinski, M., Stoll, J., Hancock, D., Robbins, J., Nattala, J., Pavelsky, T., Morrison, J., Jones, B., M.Ondrusek, Parrish, C., and the ICESat-2 Science Team: Algorithm Theoretical Basis Document (ATBD) for Along Track Inland Surface Water Data, ATL13, Release 5, https://doi.org/10.5067/RI5QTGTSVHRZ, 2021a.

Jasinski, M., Stoll, J., Hancock, D., Robbins, J., Nattala, J., Pavelsky, T., Morrison, J., Jones, B., M.Ondrusek, Parrish, C., and the ICESat-2 Science Team: ATL13 Along Track Surface Water Data, Release 004 Algorithm Notes and Known Issues, https://doi.org/10.5067/RNI05Y2CJ9FV, 2021b.

Jasinski, M., Stoll, J., Hancock, D., Robbins, J., Nattala, J., Pavelsky, T., Morrison, J., Jones, B., M.Ondrusek, Parrish, C., and the ICESat-2 Science Team: ATLAS/ICESat-2 L3A Along Track Inland Surface Water Data, Release 5, https://doi.org/10.5067/ATLAS/ATL13.005, 2021c.

Jasinski M. F., Stoll J. D., H. D. R. J. N. J. M. J. J. B. M. O. M. E. P. T. M. P. C. and the ICESat-2 Science Team: ATLAS/ICESat-2 L3A Along Track Inland Surface Water Data, Version 5, https://doi.org/https://doi.org/10.5067/ATLAS/ATL13.005, 2021.

Jiang, L., Schneider, R., Andersen, O. B., and Bauer-Gottwein, P.: CryoSat-2 Altimetry Applications over Rivers and Lakes, Water, 9, https://doi.org/10.3390/w9030211, 2017.

Jiang, L., Madsen, H., and Bauer-Gottwein, P.: Simultaneous calibration of multiple hydrodynamic model parameters using satellite altimetry observations of water surface elevation in the Songhua River, Remote Sensing of Environment, 225, 229–247, https://doi.org/10.1016/j.rse.2019.03.014, 2019.

Kittel, C. M., Hatchard, S., Neal, J. C., Nielsen, K., Bates, P. D., and Bauer-Gottwein, P.: Hydraulic model calibration using CryoSat-2 observations in the Zambezi catchment, Earth and Space Science Open Archive, p. 41, https://doi.org/10.1002/essoar.10505228.2, 2020.

Kittel, C. M. M., Jiang, L., Tøttrup, C., and Bauer-Gottwein, P.: Sentinel-3 radar altimetry for river monitoring – a catchment-scale evaluation of satellite water surface elevation from Sentinel-3A and Sentinel-3B, Hydrology and Earth System Sciences, 25, 333–357, https://doi.org/10.5194/hess-25-333-2021, 2021.

Lettenmaier, D. P., Alsdorf, D., Dozier, J., Huffman, G. J., Pan, M., and Wood, E. F.: Inroads of remote sensing into hydrologic science during the WRR era, Water Resources Research, 51, 7309–7342, https://doi.org/https://doi.org/10.1002/2015WR017616, 2015.

Li, Y., Choi, J.-I., Choic, Y., and Kim, J.: A simple and efficient outflow boundary condition for the incompressible Navier–Stokes equations, Engineering Applications of Computational Fluid Mechanics, 11, 69–85, https://doi.org/10.1080/19942060.2016.1247296, 2017.

Masson-Delmotte V., Zhai P., P. A. C. S. P. C. B. S. C. N. C. Y. G. L. G. M. H. M. L. K. L. E. M. J. M. T. W. T. Y. O. Y. R. and B.., Z.: Climate Change 2021: The Physical Science Basis. Contribution of Working Group I to the Sixth Assessment Report of the Intergovernmental Panel on Climate Change, Cambridge University Press, 6, 2021.

Nelder, J. A. and Mead, R.: A Simplex Method for Function Minimization, The Computer Journal, 7, 308–313, https://doi.org/10.1093/comjnl/7.4.308, 1965.

Neumann T. A., Brenner A., H. D. R. J. S. J. H. K. G. A. L. J. L. S. B. R. T. e. a.: ATLAS/ICESat-2 L2A Global Geolocated Photon Data, Version 5, NASA National Snow and Ice Data Center Distributed Active Archive Center, 5, https://doi.org/https://doi.org/10.5067/ATLAS/ATL03.005, 2021.

Paiva, R. C. D., Collischonn, W., Bonnet, M.-P., de Gonçalves, L. G. G., Calmant, S., Getirana, A., and Santos da Silva, J.: Assimilating in situ and radar altimetry data into a large-scale hydrologic-hydrodynamic model for streamflow forecast in the Amazon, Hydrology and Earth System Sciences, 17, 2929–2946, https://doi.org/10.5194/hess-17-2929-2013, 2013.

Paiva, R. C. D., Durand, M. T., and Hossain, F.: Spatiotemporal interpolation of discharge across a river network by using synthetic SWOT satellite data, Water Resources Research, 51, 430–449, https://doi.org/https://doi.org/10.1002/2014WR015618, 2015.

Paris, A., Dias de Paiva, R., Santos da Silva, J., Medeiros Moreira, D., Calmant, S., Garambois, P.-A., Collischonn, W., Bonnet, M.-P., and Seyler, F.: Stage-discharge rating curves based on satellite altimetry and modeled discharge in the Amazon basin, Water Resources Research, 52, 3787–3814, https://doi.org/https://doi.org/10.1002/2014WR016618, 2016.

Parrish, C. E., Magruder, L. A., Neuenschwander, A. L., Forfinski-Sarkozi, N., Alonzo, M., and Jasinski, M.: Validation of ICESat-2 AT-LAS Bathymetry and Analysis of ATLAS's Bathymetric Mapping Performance, Remote Sensing, 11, https://doi.org/10.3390/rs11141634, 2019.

Pekel, J.-F., Cottam, A., Gorelick, N., and Belward, A. S.: High-resolution mapping of global surface water and its long-term changes, Nature (London), 540, 418–422, 2016.

Ranndal, H., Andersen, O., Stenseng, L., Nielsen, K., and Knudsen, P.: CryoSat-2 altimetry for river level monitoring - Evaluation in the Ganges-Brahmaputra River basin, Remote Sensing of Environment, 168, 80–89, https://doi.org/10.1016/j.rse.2015.05.025, 2015a.

Ranndal, H., Andersen, O., Stenseng, L., Nielsen, K., and Knudsen, P.: CryoSat-2 altimetry for river level monitoring - Evaluation in the Ganges-Brahmaputra River basin, Remote Sensing of Environment, 168, 80–89, https://doi.org/10.1016/j.rse.2015.05.025, 2015b.

Saltelli, A., Tarantola, S., and Chan, K. P.-S.: A Quantitative Model-Independent Method for Global Sensitivity Analysis of Model Output, Technometrics, 41, 39–56, https://doi.org/10.1080/00401706.1999.10485594, 1999.

Shen, Y., Liu, D., Jiang, L., Yin, J., Nielsen, K., Bauer-Gottwein, P., Guo, S., and Wang, J.: On the Contribution of Satellite Altimetry-Derived Water Surface Elevation to Hydrodynamic Model Calibration in the Han River, Remote Sensing, 12, https://doi.org/10.3390/rs12244087, 2020.

Tarpanelli, A., Camici, S., Nielsen, K., Brocca, L., Moramarco, T., and Benveniste, J.: Potentials and limitations of Sentinel-3 for river discharge assessment, Advances in Space Research, 68, 593–606, https://doi.org/https://doi.org/10.1016/j.asr.2019.08.005, 25 Years of Progress in Radar Altimetry, 2021.

Vrugt, J. A.: Markov chain Monte Carlo simulation using the DREAM software package: Theory, concepts, and MATLAB implementation, Environmental Modelling Software, 75, 273–316, https://doi.org/https://doi.org/10.1016/j.envsoft.2015.08.013, 2016.

Xu, N., Zheng, H., Ma, Y., Yang, J., Liu, X., and Wang, X.: Global Estimation and Assessment of Monthly Lake/Reservoir Water Level Changes Using ICESat-2 ATL13 Products, Remote Sensing, 13, https://doi.org/10.3390/rs13142744, 2021.

530 Yamazaki D., D. Ikeshima, J. S. P. B. G. A. T. P.: MERIT Hydro: A high-resolution global hydrography map based on latest topography datasets, Water Resources Research, 55, pp.5053–5073, https://doi.org/10.1029/2019WR024873, 2019.

Yoon, Y., Durand, M., Merry, C., and Rodriguez, E.: Improving Temporal Coverage of the SWOT Mission Using Spatiotemporal Kriging, Selected Topics in Applied Earth Observations and Remote Sensing, IEEE Journal of, 6, 1719–1729, https://doi.org/10.1109/JSTARS.2013.2257697, 2013.